Int j simul model 24 (2025) 2, 321-332
Original scientific paper

A NOVEL TRANSITIONAL ELEMENT-BASED APPROACH FOR PD-FEM COUPLING: THEORETICAL DEVELOPMENT

Liu, Z. L.[#]; Chen, X. Y. & Cheng, W. D.
School of Mechanical, Electronic and Control Engineering, Beijing Jiaotong University, Beijing 100044, P. R. China
E-Mail: liuzhl@bjtu.edu.cn ([#] Corresponding author)

Abstract
Peridynamics (PD) has emerged as a powerful computational method for modelling discontinuities, but its inherent surface effects and computational inefficiencies limit its standalone application. The Finite Element Method (FEM), while effective for boundary conditions, struggles with crack propagation modelling. This paper proposes a novel Transitional Element (TE)-based framework to seamlessly couple PD and FEM, ensuring computational compatibility and efficiency. By introducing a stiffness matrix correction approach, the TE mitigates interface inconsistencies and enhances accuracy. The proposed method preserves the strengths of both PD and FEM while significantly reducing computational cost. This framework lays a solid foundation for future applications in fracture mechanics and material failure analysis.
(Received in January 2025, accepted in April 2025. This paper was with the authors 1 month for 1 revision.)

Key Words: Peridynamics, FEM, Coupling Model, Compatibility, Transitional Element, Stiffness Matrix Correction

1. INTRODUCTION

Peridynamics (PD) is a nonlocal continuum mechanics theory proposed by Silling in 2000 [1], particularly suitable for simulating discontinuous problems. PD employs integral equations to describe material behaviour, thereby avoiding the limitations of classical continuum mechanics when dealing with singularities (e.g., crack tips) [2]. However, the nonlocal nature of PD results in high computational cost [3] and surface effects near the boundary [4], which affect the accuracy. In contrast, FEM is a well-established local method with significant advantages in computational efficiency and boundary condition handling [5]. Therefore, coupling PD with FEM has emerged as a promising strategy, enabling the utilization of PD's strengths in discontinuous regions while leveraging FEM's efficiency in continuous regions.

In order to achieve effective coupling between PD and FEM, researchers have proposed various strategies, mainly addressing the incompatibilities between the non-local PD region and the local FEM region. The overlapping method is one of the earliest proposed coupling strategies. This method forms an overlapping region of PD and FEM, within which both methods are applied simultaneously. For example, Han and Lubineau [6] coupled PD and FEM by using the Arlequin method to ensure energy consistency in the overlapping area. Yu et al. [7] derived the weak form of the motion equation for the hybrid model by applying Hamilton's principle. Pernatii et al. [8] developed coupling equations of the overlapping zone with help of the penalty method. The overlapping method is able to ensure a smooth transition between the PD and FEM regions, but requires careful adjustment of the overlapping regions and the transitional functions. Another strategy is to define a well-defined boundary between PD and FEM regions and ensure continuity through specific interface conditions. For example, Galvanetto et al. [9] and Zaccariotto et al. [10] proposed an innovative strategy that effectively couples PD grids with FEM, in which no arbitrary choice or tuning of parameters or blending functions are required. Anicode and Madenci [11] employed the concept of dual horizon PD to enable the PD and FEM regions to share the same nodes along the interface

without an overlap zone. This type of method avoids the need for overlapping regions, but requires precise processing at the interface to guarantee accuracy. In recent years, adaptive methods have also received attention. In this type of method, the PD and FEM regions can be dynamically adjusted according to the evolution of the solution (such as crack propagation). Ou et al. [12] developed an adaptive coupling model based on the morphing method, effectively improving the computing efficiency. Dong et al. [13] introduced an adaptive transition criterion to ensure that the sub-regions automatically evolve as the crack grows, thus eliminating the need for prior knowledge of the crack propagation path. Liu et al. [14] presented an adaptive coupling PD least-square minimization with FEM for fracture analysis while minimizing the PD region for computational efficiency. This strategy is especially suitable for complex problems with unknown crack paths. However, it also increases the complexity of updating the computational regions and ensuring simulation stability.

The above coupling methods offer valuable insights for coupling PD and FEM. However, the current coupling models still have some issues, such as the need for complex functions or methods to handle interface or overlapping regions, certain requirements on the types of PD models or finite elements involved in the coupling, and the resulting complexity in the numerical implementation. In order to address these issues to fully realize the potential of PD-FEM hybrid models, this paper proposes a new coupling framework based on the concept of "Transitional Element (TE)". The Transitional Elements consist of PD nodes and FEM nodes located at the interface of PD and FEM, serving to connect these two areas. The TE stiffness matrix can be obtained by simply adjusting the original FEM stiffness matrix. The specific form of the transitional element can vary depending on the problem. This characteristic enables it to be applicable to a wide range of problems. It imposes no specific requirements on the types of finite elements or PD elements, thus allowing for easy implementation of coupling between various types of PD and FEM elements and enables solutions within a unified finite element framework. Consequently, it effectively addresses some limitations inherent in other methods and lays a solid foundation for fully leveraging the advantages of both PD and FEM, as well as facilitating their practical applications in engineering problems.

2. BASIC THEORY OF PERIDYNAMICS

The core innovation of PD theory is that it no longer relies on local differential equations to describe the constitutive relations within materials. Instead, PD employs integral equations to describe the non-local constitutive relationships between material points, meaning that the behaviour of each point is influenced by multiple points within a certain range around it, as illustrated in Fig. 1. The introduction of this non-local interaction enables PD to more effectively handle crack propagation and fracture problems, especially in complex situations.

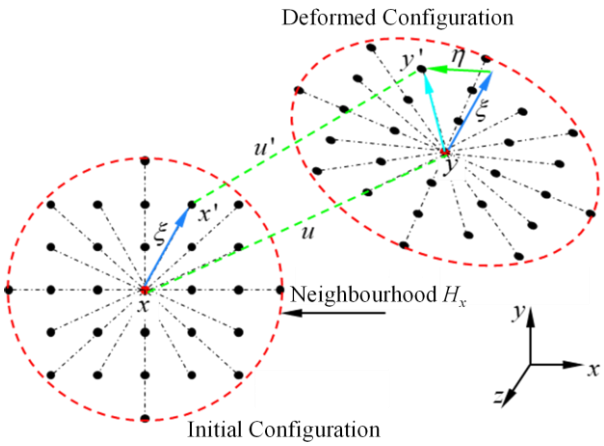

Figure 1: The non-local interaction and deformation in PD.

The PD integral equation for a material point within the body can be expressed as:

$$\rho(x)\ddot{u}(x,t) = \int_{H_x} f(\eta,\xi,t)\,dV_{X'} + b(x,t) \quad \forall x \in \Omega, t \geq 0 \tag{1}$$

where ρ represents the material density, $\ddot{u}$ is the acceleration of the material point x at time t, and x, x' represent the current material point and its neighbouring point, respectively. $b(x, t)$ denotes the external body force density. H_x represents the integral domain centred at material point x, which consists of the neighbouring points within its neighbourhood, expressed as:

$$H_x = \{x' \in \Omega: \ |x' - x| \leq \delta\} \tag{2}$$

δ is defined as the horizon of the material point in PD. In Eq. (1), f is called constitutive force function of the bond, representing the bond force density between the pair of material points, mainly influenced by bond deformation. The integral term represents the total nonlocal forces exerted on material point x by all neighbouring points within its neighbourhood H_x. ξ is defined as the initial bond between material point x and its neighbouring point x', expressed as:

$$\xi = x' - x, \quad x' \in H_x \tag{3}$$

where η is the relative displacement of the bond between material point x and x' after deformation, expressed as:

$$\eta = u'(x',t) - u(x,t) \tag{4}$$

where $u(x, t)$ and $u'(x', t)$ are the displacements of material point x and x', respectively.

In PD, the PMB (Pairwise Force Material Bond) material constitutive model is typically used to define the interaction relationships between material points. Its constitutive force function can be expressed as:

$$f = c\mu s\frac{\xi + \eta}{|\xi + \eta|} \tag{5}$$

where f represents the non-local force density exerted on the central point x by the material points in the neighbourhood, also referred to as bond force or constitutive force between material points. c denotes the micro-modulus, representing the stiffness of the bond [15]. s represents the elongation rate of the bond, which is expressed as:

$$s = \frac{|\xi + \eta| - |\xi|}{|\xi|} \tag{6}$$

where $|\xi|$ is the length of the bond before deformation, and $|\xi+\eta|$ is the length of the bond after deformation. μ is defined as a time-varying scalar function used to assess the status of bonds between material points within the material. This function is typically employed to describe whether a bond has fractured and the extent of damage. For any given time period, from 0 to t ($0 \leq t' \leq t$), the scalar function used to assess bond status is defined as follow:

$$\mu(\xi,\ t) = \begin{cases} 1, & \mu(\xi,\ t') < s_c \\ 0, & \mu(\xi,\ t') \geq s_c \end{cases} \tag{7}$$

where 0 represents the state where the bond is completely undamaged, while 1 indicates that the bond has fractured. s_c represents the critical elongation rate, which is used to describe the failure threshold of the bond. When multiple fractured bonds are aligned consecutively, they form a clear path, and this is how PD can naturally describe cracks.

3. METHODOLOGY

3.1 Introduction of the Transitional Element concept

To eliminate the inherent "surface effect" in PD, coupling with FEM offers an effective approach. By setting the boundary of the object as the FEM region, FEM will surround the

PD boundary, ensuring that even the outermost PD nodes have a complete neighbourhood. This configuration avoids "surface effect", as shown in Fig. 2 a. The region near the boundary is set as FEM region, including nodes 1 and 2. Then, the node on the boundary of the PD region, such as node 3, has a complete neighbourhood. However, coupling at this stage is not sufficient, as it may result in incomplete forces on the FEM nodes (e.g., node 2 in Fig. 2 a) adjacent to the PD region, as these nodes are internal nodes and should also be subjected to local forces from PD nodes. Therefore, it is necessary to include the local actions from the PD nodes on the adjacent FEM nodes to preserve force equilibrium, as illustrated in Fig. 2 b. One way to address this is to add FEM elements between FEM and PD nodes. However, this also introduces redundant local interactions on the PD nodes, e.g., node 3 in Fig. 2 c, which is simultaneously subjected to both local and non-local influences from node 2. Consequently, further adjustment to these elements is needed: retaining only the local actions on FEM nodes and removing those affecting the PD nodes. This type of element, used to connect the PD and FEM regions, is the "Transitional Element (TE)" newly proposed in this paper, as illustrated in Fig. 2 d, which is equivalent to Fig. 2 b. The setup of TE addresses the harmonization of local and non-local interactions at the interface of PD and FEM regions.

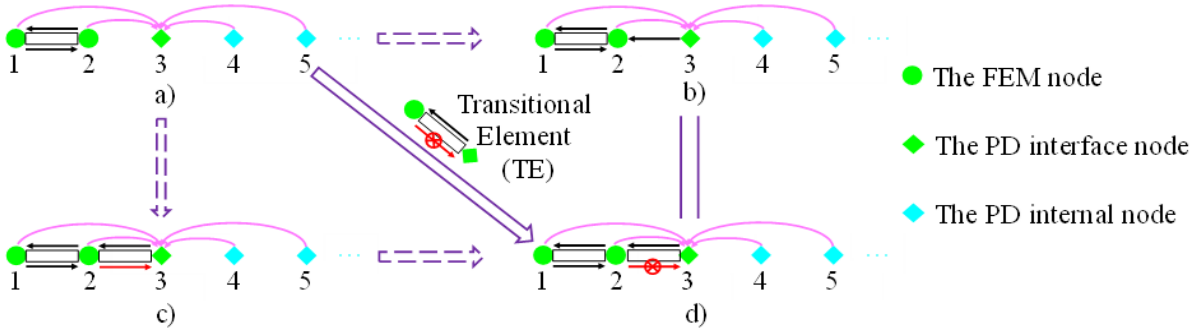

Figure 2: Illustration of the "Transitional Element (TE)" setup process.

3.2 Derivation of the PD-FEM coupling framework based on the Transitional Element

For clarity reason, the new coupling method is presented with the help of the above 1D example.

First, consider fully using the PD method to solve the problem. For consistency in subsequent calculations, the finite element formulation of the PD method is applied here. Based on the principle of minimum potential energy, a form of the stiffness matrix for the finite element discretization of PD was derived, as detailed in the references [16, 17]:

$$k_i^{PD} = \begin{bmatrix} \left(\frac{\partial^2 E_{(i)}^{PD}}{\partial x_{(i)} \partial x_{(i)}}\right)_{n\times n} & \left(\frac{1}{2}\frac{\partial^2 E_{(i)}^{PD}}{\partial x_{(i)} \partial x_{(j)}}\right)_{n\times Mn} \\ \left(\frac{1}{2}\frac{\partial^2 E_{(i)}^{PD}}{\partial x_{(j)} \partial x_{(i)}}\right)_{Mn\times n} & (0)_{Mn\times Mn} \end{bmatrix} \tag{8}$$

where k_i^{PD} is the finite element formation of the non-local stiffness matrix of PD, and the corresponding non-equilibrium force vector P_i^{PD} can be expressed as:

$$P_i^{PD} = \begin{bmatrix} (-\frac{\partial E_{(i)}^{PD}}{\partial x_{(i)}})_{n\times 1} \\ (0)_{Mn\times 1} \end{bmatrix} \tag{9}$$

where $E_{(i)}^{PD}$ is the total potential energy associated with the node $X_{(i)}$:

$$E_{(i)}^{PD}(x) = \sum_{j=1}^{M} \frac{1}{2} c s_{(i)(j)}^2 |X_{(j)} - X_{(i)}| v_{c(j)} V_{(i)} V_{(j)} - b_{(i)} u_{(i)} V_{(i)} \tag{10}$$

where M represents the number of neighbouring nodes within the horizon radius of $X_{(i)}$, n represents the spatial dimensions of the model. $V_{(i)}$ and $V_{(j)}$ represent the volume of the node $X_{(i)}$ and $X_{(j)}$, respectively; $u_{(i)}$ and $b_{(i)}$ represent the displacement and body force density of the node $X_{(i)}$, respectively, and $v_{c(j)}$ is the volume correction coefficient [18].

However, the form of Eq. (8) is not suitable for the matrix coupling, as it requires additional treatment for all the PD interface nodes. In fact, unlike the traditional FEM, the i^{th} row of the stiffness matrix and the i^{th} component of the non-equilibrium force vector P in PD are entirely determined by the single PD element centred at node i [16], then the element stiffness matrix for node i in PD can be expressed as:

$$k_i^{PD} = \begin{bmatrix} (0)_{(M/2)n\times(M/2)n} & (0)_{(M/2)n\times n} & (0)_{(M/2)n\times(M/2)n} \\ \left(\frac{\partial^2 E_{(i)}^{PD}}{\partial x_{(j)}\partial x_{(i)}}\right)_{n\times(M/2)n} & \left(\frac{\partial^2 E_{(i)}^{PD}}{\partial x_{(i)}\partial x_{(i)}}\right)_{n\times n} & \left(\frac{\partial^2 E_{(i)}^{PD}}{\partial x_{(i)}\partial x_{(j)}}\right)_{n\times(M/2)n} \\ (0)_{(M/2)n\times(M/2)n} & (0)_{(M/2)n\times n} & (0)_{(M/2)n\times(M/2)n} \end{bmatrix} \tag{11}$$

and the corresponding non-equilibrium force vector P_i^{PD} is accordingly adjusted to:

$$P_i^{PD} = \begin{bmatrix} (0)_{(M/2)n\times 1} \\ \left(-\frac{\partial E_{(i)}^{PD}}{\partial x_{(i)}}\right)_{n\times 1} \\ (0)_{(M/2)n\times 1} \end{bmatrix} \tag{12}$$

It should be emphasized that the form of the PD element stiffness matrix represented by Eq. (11) applies to all elements within the PD region, regardless of whether they are located in the interior or on the interface. This eliminates the need for special treatment of interface nodes when coupling PD with traditional FEM stiffness matrices, thereby facilitating the construction of the coupling model.

For the 1D model shown in Fig. 2, each central node has 4 neighbouring nodes, then Eq. (11) can be simplified as follows:

$$k_i^{PD} = \begin{bmatrix} 0 & 0 & 0 & 0 & 0 \\ 0 & 0 & 0 & 0 & 0 \\ k_{i,-2}^{PD} & k_{i,-1}^{PD} & k_{i,0}^{PD} & k_{i,+1}^{PD} & k_{i,+2}^{PD} \\ 0 & 0 & 0 & 0 & 0 \\ 0 & 0 & 0 & 0 & 0 \end{bmatrix} \tag{13}$$

where $\boldsymbol{k_{i,j}^{PD}}$ (j = 0, -1, -2, +1, +2) represents the central term and its surrounding terms of the element stiffness matrix corresponding to the i^{th} PD node. By assembling the stiffness matrix of each node, the global stiffness matrix of the 1D model shown in Fig. 2 can be obtained:

$$[K] = K^{PD} = \begin{array}{c} \begin{bmatrix} u_1 & u_2 & u_3 & u_4 & u_5 & \dots & \dots & \dots & \dots \end{bmatrix} \\ \begin{bmatrix} k_{1,0}^{PD} & k_{1,+1}^{PD} & k_{1,+2}^{PD} & 0 & 0 & 0 & 0 & 0 & 0 \\ k_{2,-1}^{PD} & k_{2,0}^{PD} & k_{2,+1}^{PD} & k_{2,+2}^{PD} & 0 & 0 & 0 & 0 & 0 \\ k_{3,-2}^{PD} & k_{3,-1}^{PD} & k_{3,0}^{PD} & k_{3,+1}^{PD} & k_{3,+2}^{PD} & 0 & 0 & 0 & 0 \\ 0 & k_{4,-2}^{PD} & k_{4,-1}^{PD} & k_{4,0}^{PD} & k_{4,+1}^{PD} & k_{4,+2}^{PD} & 0 & 0 & 0 \\ 0 & 0 & k_{5,-2}^{PD} & k_{5,-1}^{PD} & k_{5,0}^{PD} & k_{5,+1}^{PD} & k_{5,+2}^{PD} & 0 & 0 \\ 0 & 0 & 0 & \dots & \dots & \dots & \dots & \dots & 0 \\ 0 & 0 & 0 & 0 & \dots & \dots & \dots & \dots & \dots \\ 0 & 0 & 0 & 0 & 0 & \dots & \dots & \dots & \dots \\ 0 & 0 & 0 & 0 & 0 & 0 & \dots & \dots & \dots \end{bmatrix} \end{array} \begin{array}{c} \\ \begin{bmatrix} u_1 \\ u_2 \\ u_3 \\ u_4 \\ u_5 \\ \dots \\ \dots \\ \dots \\ \dots \end{bmatrix} \end{array} \tag{14}$$

where u_1~u_5, … represent the degrees of freedom corresponding to nodes 1~5, …

Next, consider fully using the FEM method to solve the problem. For the 1D structure shown in Fig. 2, the entire model can be discretized using rod elements The general expression of stiffness matrix for a two-node linear rod element is given by [19]:

$$k_i^{FEM} = \begin{bmatrix} k_{i,11}^{FEM} & k_{i,12}^{FEM} \\ k_{i,21}^{FEM} & k_{i,22}^{FEM} \end{bmatrix} \tag{15}$$

where $\boldsymbol{k_i^{FEM}}$ is the stiffness matrix for the i^{th} element. $\boldsymbol{k_{i,11}^{FEM}, k_{i,12}^{FEM}, k_{i,21}^{FEM}, k_{i,22}^{FEM}}$ represent the terms at different positions in the i^{th} element stiffness matrix. By assembling the stiffness matrix of each rod element, the global stiffness matrix of the 1D model shown in Fig. 2 can be obtained:

$$[K] = K^{FEM} = \begin{array}{c} \begin{matrix} u_1 & u_2 & u_3 & u_4 & u_5 & \dots & \dots & \dots & \dots \end{matrix} \\ \begin{bmatrix} k_{1,11}^{FEM} & k_{1,12}^{FEM} & 0 & 0 & 0 & 0 & 0 & 0 & 0 \\ k_{1,21}^{FEM} & k_{1,22}^{FEM} + k_{2,11}^{FEM} & k_{2,12}^{FEM} & 0 & 0 & 0 & 0 & 0 & 0 \\ 0 & k_{2,21}^{FEM} & k_{2,22}^{FEM} + k_{3,11}^{FEM} & k_{3,12}^{FEM} & 0 & 0 & 0 & 0 & 0 \\ 0 & 0 & k_{3,21}^{FEM} & k_{3,22}^{FEM} + k_{4,11}^{FEM} & k_{4,12}^{FEM} & 0 & 0 & 0 & 0 \\ 0 & 0 & 0 & k_{4,21}^{FEM} & k_{4,22}^{FEM} + k_{5,11}^{FEM} & k_{5,12}^{FEM} & 0 & 0 & 0 \\ 0 & 0 & 0 & 0 & k_{5,21}^{FEM} & k_{5,22}^{FEM} & \dots & 0 & 0 \\ 0 & 0 & 0 & 0 & 0 & \dots & \dots & \dots & 0 \\ 0 & 0 & 0 & 0 & 0 & 0 & \dots & \dots & \dots \\ 0 & 0 & 0 & 0 & 0 & 0 & 0 & \dots & \dots \end{bmatrix} \end{array} \begin{matrix} u_1 \\ u_2 \\ u_3 \\ u_4 \\ u_5 \\ \dots \\ \dots \\ \dots \\ \dots \end{matrix} \tag{16}$$

Subsequently, the coupling of the two methods is taken into consideration. In the coupling scheme depicted in Fig. 2 a, wherein points 1 and 2 are treated as FEM nodes and points 3, 4, and 5, ... as PD nodes, the global stiffness matrix can be formulated by appropriately extracting and assembling the corresponding submatrices from Eqs. (14) and (16), in strict adherence to the principle of stiffness invariance under the mapping of nodal degrees of freedom. Thus, the global stiffness matrix of the coupling model is given by:

$$[K] = \begin{array}{c} \begin{matrix} u_1 & u_2 & u_3 & u_4 & u_5 & \dots & \dots & \dots & \dots \end{matrix} \\ \begin{bmatrix} k_{1,11}^{FEM} & k_{1,12}^{FEM} & 0 & 0 & 0 & 0 & 0 & 0 & 0 \\ k_{1,21}^{FEM} & k_{1,22}^{FEM} + k_{2,11}^{FEM} & k_{2,12}^{FEM} & 0 & 0 & 0 & 0 & 0 & 0 \\ k_{3,-2}^{PD} & k_{3,-1}^{PD} & k_{3,0}^{PD} & k_{3,+1}^{PD} & k_{3,+2}^{PD} & 0 & 0 & 0 & 0 \\ 0 & k_{4,-2}^{PD} & k_{4,-1}^{PD} & k_{4,0}^{PD} & k_{4,+1}^{PD} & k_{4,+2}^{PD} & 0 & 0 & 0 \\ 0 & 0 & k_{5,-2}^{PD} & k_{5,-1}^{PD} & k_{5,0}^{PD} & k_{5,+1}^{PD} & k_{5,+2}^{PD} & 0 & 0 \\ 0 & 0 & 0 & \dots & \dots & \dots & \dots & \dots & 0 \\ 0 & 0 & 0 & 0 & \dots & \dots & \dots & \dots & \dots \\ 0 & 0 & 0 & 0 & 0 & \dots & \dots & \dots & \dots \\ 0 & 0 & 0 & 0 & 0 & 0 & \dots & \dots & \dots \end{bmatrix} \end{array} \begin{matrix} u_1 \\ u_2 \\ u_3 \\ u_4 \\ u_5 \\ \dots \\ \dots \\ \dots \\ \dots \end{matrix} \tag{17}$$

Moreover, this stiffness matrix can be interpreted as the assembly of the following three constituent matrices:

$$K^1 = \begin{array}{c} \begin{matrix} u_1 & u_2 \end{matrix} \\ \begin{bmatrix} k_{1,11}^{FEM} & k_{1,12}^{FEM} \\ k_{1,21}^{FEM} & k_{1,22}^{FEM} \end{bmatrix} \end{array} \begin{matrix} u_1 \\ u_2 \end{matrix} \tag{18}$$

$$K^2 = \begin{array}{c} \begin{matrix} u_2 & u_3 \end{matrix} \\ \begin{bmatrix} k_{2,11}^{FEM} & k_{2,12}^{FEM} \\ 0 & 0 \end{bmatrix} \end{array} \begin{matrix} u_2 \\ u_3 \end{matrix} \tag{19}$$

$$K^3 = \begin{bmatrix} u_1 & u_2 & u_3 & u_4 & u_5 & \dots & \dots & \dots & \dots \\ 0 & 0 & 0 & 0 & 0 & 0 & 0 & 0 & 0 \\ 0 & 0 & 0 & 0 & 0 & 0 & 0 & 0 & 0 \\ k_{3,-2}^{PD} & k_{3,-1}^{PD} & k_{3,0}^{PD} & k_{3,+1}^{PD} & k_{3,+2}^{PD} & 0 & 0 & 0 & 0 \\ 0 & k_{4,-2}^{PD} & k_{4,-1}^{PD} & k_{4,0}^{PD} & k_{4,+1}^{PD} & k_{4,+2}^{PD} & 0 & 0 & 0 \\ 0 & 0 & k_{5,-2}^{PD} & k_{5,-1}^{PD} & k_{5,0}^{PD} & k_{5,+1}^{PD} & k_{5,+2}^{PD} & 0 & 0 \\ 0 & 0 & 0 & \dots & \dots & \dots & \dots & \dots & 0 \\ 0 & 0 & 0 & 0 & \dots & \dots & \dots & \dots & \dots \\ 0 & 0 & 0 & 0 & 0 & \dots & \dots & \dots & \dots \\ 0 & 0 & 0 & 0 & 0 & 0 & \dots & \dots & \dots \end{bmatrix} \begin{matrix} u_1 \\ u_2 \\ u_3 \\ u_4 \\ u_5 \\ \dots \\ \dots \\ \dots \\ \dots \end{matrix} \tag{20}$$

Specifically, Eq. (18) represents the stiffness matrix of the FEM region formed by nodes 1 and 2, while Eq. (20) corresponds to the stiffness matrix of the PD region consisting of nodes 3, 4, 5, etc. Eq. (19), on the other hand, represents a stiffness matrix that can be interpreted as the finite element stiffness matrix associated with nodes 2 and 3, from which the components corresponding to the degrees of freedom of the PD nodes have been removed. The element represented by Eq. (19) effectively connects the FEM and PD regions, serving as a transitional interface; hence, it is referred to as a "Transitional Element (TE)".

The construction of the TE stiffness matrix is the key to this coupling method. From the above derivation of the TE stiffness matrix, it can be observed that the transitional element consists of FEM nodes and PD nodes located at the interface. The construction of the TE stiffness matrix can be summarized in the following two steps:

(i) Firstly, treat the transitional element composed of FEM and PD interface nodes as a traditional FEM element and formulate its stiffness matrix;

(ii) Secondly, set the components corresponding to the degrees of freedom of the PD nodes to zero.

Therefore, the TE stiffness matrix k_e^{TE} has the following concise general expression:

$$k_e^{TE} = \begin{bmatrix} \dots \\ (k_{pq})_{n\times Ln} \\ (0)_{n\times Ln} \\ \dots \end{bmatrix}_{Ln\times Ln} \begin{matrix} \\ \Leftarrow \text{ FEM node} \\ \Leftarrow \text{ PD node} \\ \\ \end{matrix} \quad \text{where} \quad p, q = (1, 2, 3, \dots, Ln) \tag{21}$$

where $(k_{pq})_{n\times Ln}$ represent the terms in the original FEM element stiffness matrix corresponding to the FEM nodes, while $(0)_{n\times Ln}$ correspond to the PD nodes. L is the number of nodes contained in a transitional element, and n is the number of degrees of freedom per node.

The specific form of the transitional element varies depending on the problem's dimensionality, as well as the number and positions of the FEM and PD nodes it contains. This characteristic of the TE enables it to be applicable to a wide range of problems while maintaining, as much as possible, the independence between the FEM and PD regions.

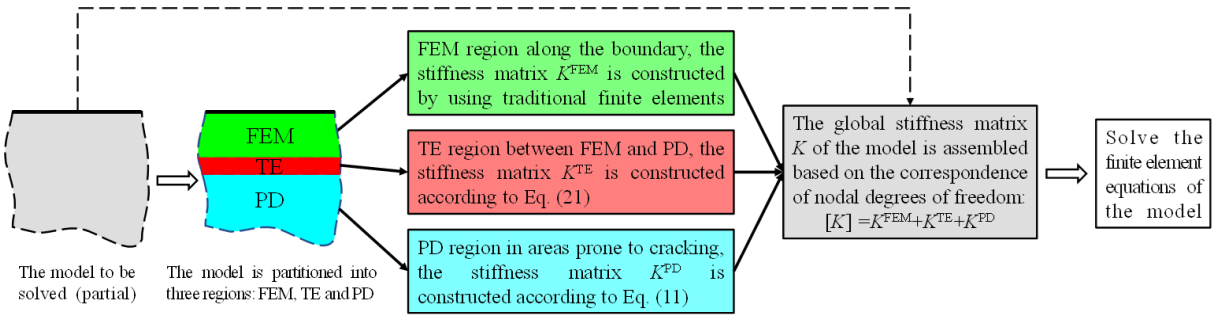

Figure 3: The novel PD-FEM coupling framework based on the "Transitional Element (TE)".

Through the above derivation and analysis, the novel PD-FEM coupling framework based on the "Transitional Element (TE)" can be described as follows (Fig. 3). The entire solution domain is divided into three non-overlapping yet closely connected subdomains: FEM, TE and PD. The FEM subdomain is located at the structural boundaries to mitigate boundary effects and to save computational resources. The PD subdomain is designated for regions susceptible to discontinuities, such as crack formation and growth. And the TE subdomain, consists of the interface nodes of PD and FEM, connecting the two. Within this framework, the TE elements facilitate the coupling of the two subdomains while maximally preserving their independence, thereby enabling full utilization of the strengths of both methods.

For the convenience of calculation consistency, the three subdomains can be uniformly solved using the finite element method. In the framework established above, the equilibrium equation of the coupling model can be expressed as:

$$[F]_{N\times 1} = [K]_{N\times N}[U]_{N\times 1} \tag{22}$$

where N is the total degrees of freedom of the system, $[F]_{N\times 1}$ represents the total nodal load of the coupling model, expressed as:

$$[F]_{N\times 1} = [f_1, \quad f_2, \quad f_3, \quad \ldots, \quad f_N]^T \tag{23}$$

and $[U]_{N\times 1}$ is the global displacement matrix of the coupling model, expressed as:

$$[U]_{N\times 1} = [u_1, \quad u_2, \quad u_3, \quad \ldots, \quad u_N]^T \tag{24}$$

The global stiffness matrix $[K]_{N\times N}$ of the coupling model can be expressed as:

$$[K]_{N\times N} = \sum_{e=1}^{N^{FEM}} k_e^{FEM} + \sum_{e=1}^{N^{TE}} k_e^{TE} + \sum_{i=1}^{N^{PD}} k_i^{PD} \tag{25}$$

where k_e^{FEM} is the stiffness matrix of FEM, and N^{FEM} is the number of traditional finite elements; k_e^{TE} is the stiffness matrix of TE, which is constructed according to Eq. (21), and N^{TE} is the number of transitional elements; k_i^{PD} is the stiffness matrix of PD, which is constructed according to Eq. (11), and N^{PD} is the number of nodes in the PD subdomain.

3.3 Validation and discussion

To further demonstrate the construction of the framework and provide a preliminary validation, a simple case study is carried out on a 1D coupled model (Fig. 4). This model includes FEM nodes (green circle) on the boundary, which are connected by rod finite elements of black rectangular, forming the FEM subdomain. The light blue square represents the PD internal nodes, which are connected by purple thin curves (PD bond), forming the PD subdomain. The transitional elements (red rectangular) connect the two subdomains.

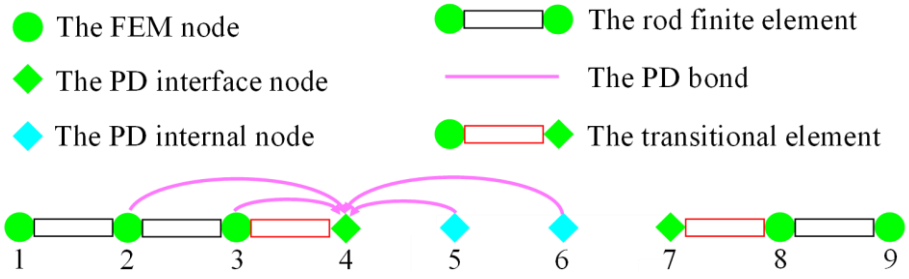

Figure 4: 1D PD-FEM coupling model.

In the 1D model, based on the position of the PD interface node within the TE, the transitional elements can be divided into two types: Type 1, composed of nodes 3 and 4, and Type 2, composed of nodes 7 and 8 in Fig. 4. The TE stiffness matrix can be derived by

modifying the finite element stiffness matrix. To eliminate the local interaction of adjacent FEM nodes on the PD nodes, one only needs to zero out the rows of the TE stiffness matrix corresponding to the degrees of freedom associated with the PD nodes. The finite element stiffness matrix for a two-node linear rod element is given by [19]:

$$k_{rod}^{FEM} = \frac{EA}{\Delta x}\begin{bmatrix} 1 & -1 \\ -1 & 1 \end{bmatrix} = a\begin{bmatrix} 1 & -1 \\ -1 & 1 \end{bmatrix} \qquad \text{where} \quad a = \frac{EA}{\Delta x} \tag{26}$$

where E is the Young's modulus, A is the area of the cross section and Δx is the length of the finite element. Then, the stiffness matrix for TE of Type 1 is:

$$k_1^{TE} = a\begin{bmatrix} 1 & -1 \\ 0 & 0 \end{bmatrix} \tag{27}$$

The stiffness matrix for TE of Type 2 is:

$$k_2^{TE} = a\begin{bmatrix} 0 & 0 \\ -1 & 1 \end{bmatrix} \tag{28}$$

Therefore, the stiffness matrix K^{TE} of the TE subdomain composed of nodes 3, 4, 7, and 8 is:

$$K^{TE} = \sum_{e=1}^{2} k_e^{TE} = \begin{array}{c} \begin{matrix} u_3 & u_4 & u_7 & u_8 \end{matrix} \\ \begin{bmatrix} a & -a & 0 & 0 \\ 0 & 0 & 0 & 0 \\ 0 & 0 & 0 & 0 \\ 0 & 0 & -a & a \end{bmatrix} \end{array} \begin{matrix} u_3 \\ u_4 \\ u_7 \\ u_8 \end{matrix} \tag{29}$$

where u_1~u_9 represent the degrees of freedom corresponding to nodes 1 to 9.

It can be easily derived that the stiffness matrix K^{FEM} of the FEM subdomain composed of nodes 1, 2, 3, 8, and 9 is:

$$K^{FEM} = \sum_{e=1}^{3} k_e^{FEM} = \begin{array}{c} \begin{matrix} u_1 & u_2 & u_3 & u_8 & u_9 \end{matrix} \\ \begin{bmatrix} a & -a & 0 & 0 & 0 \\ -a & 2a & -a & 0 & 0 \\ 0 & -a & a & 0 & 0 \\ 0 & 0 & 0 & a & -a \\ 0 & 0 & 0 & -a & a \end{bmatrix} \end{array} \begin{matrix} u_1 \\ u_2 \\ u_3 \\ u_8 \\ u_9 \end{matrix} \tag{30}$$

According to Eq. (11), the stiffness matrix of the PD element centred at node 4 is:

$$k_4^{PD} = \begin{array}{c} \begin{matrix} u_2 & u_3 & u_4 & u_5 & u_6 \end{matrix} \\ \begin{bmatrix} 0 & 0 & 0 & 0 & 0 \\ 0 & 0 & 0 & 0 & 0 \\ -0.25b & -b & 2.5b & -b & -b \\ 0 & 0 & 0 & 0 & 0 \\ 0 & 0 & 0 & 0 & 0 \end{bmatrix} \end{array} \begin{matrix} u_2 \\ u_3 \\ u_4 \\ u_5 \\ u_6 \end{matrix} \tag{31}$$

where $b = cV_{(i)}V_{(j)}/r_{(i)(j)}^0$, $r_{(i)(j)}^0$ is the uniform distance between two adjacent nodes. The stiffness matrix of the PD elements entered at nodes 5, 6, and 7 have the similar expressions as above. Assembling the element stiffness matrix of the PD subdomain yields the stiffness matrix of the PD subdomain as follows:

$$K^{PD} = \sum_{i=4}^{7} k_i^{PD} = \begin{array}{c} \begin{matrix} u_2 & u_3 & u_4 & u_5 & u_6 & u_7 & u_8 & u_9 \end{matrix} \\ \begin{bmatrix} 0 & 0 & 0 & 0 & 0 & 0 & 0 & 0 \\ 0 & 0 & 0 & 0 & 0 & 0 & 0 & 0 \\ -0.25b & -b & 2.5b & -b & -0.25b & 0 & 0 & 0 \\ 0 & -0.25b & -b & 2.5b & -b & -0.25b & 0 & 0 \\ 0 & 0 & -0.25b & -b & 2.5b & -b & -0.25b & 0 \\ 0 & 0 & 0 & -0.25b & -b & 2.5b & -b & -0.25b \\ 0 & 0 & 0 & 0 & 0 & 0 & 0 & 0 \\ 0 & 0 & 0 & 0 & 0 & 0 & 0 & 0 \end{bmatrix} \end{array} \begin{matrix} u_2 \\ u_3 \\ u_4 \\ u_5 \\ u_6 \\ u_7 \\ u_8 \\ u_9 \end{matrix} \tag{32}$$

Then, by assembling the stiffness matrices of FEM, TE, and PD elements, the global stiffness matrix is formed as follows:

$$[K] = K^{FEM} + K^{TE} + K^{PD} = \begin{array}{c} \begin{matrix} u_1 & u_2 & u_3 & u_4 & u_5 & u_6 & u_7 & u_8 & u_9 \end{matrix} \\ \begin{bmatrix} a & -a & 0 & 0 & 0 & 0 & 0 & 0 & 0 \\ -a & 2a & -a & 0 & 0 & 0 & 0 & 0 & 0 \\ 0 & -a & 2a & -a & 0 & 0 & 0 & 0 & 0 \\ 0 & -0.25b & -b & 2.5b & -b & -0.25b & 0 & 0 & 0 \\ 0 & 0 & -0.25b & -b & 2.5b & -b & -0.25b & 0 & 0 \\ 0 & 0 & 0 & -0.25b & -b & 2.5b & -b & -0.25b & 0 \\ 0 & 0 & 0 & 0 & -0.25b & -b & 2.5b & -b & -0.25b \\ 0 & 0 & 0 & 0 & 0 & 0 & -a & 2a & -a \\ 0 & 0 & 0 & 0 & 0 & 0 & 0 & -a & a \end{bmatrix} \end{array} \begin{matrix} u_1 \\ u_2 \\ u_3 \\ u_4 \\ u_5 \\ u_6 \\ u_7 \\ u_8 \\ u_9 \end{matrix} \quad (33)$$

The 1D form of the global stiffness matrix expressed in Eq. (33) is consistent with Eq. (13) in Ref. [9], which provides evidence for the correctness of the method from one perspective.

In this example, the left end of the model is fixed, while a horizontal external load is applied at the right end. By substituting the parameters listed in Table I into the model, the numerical results shown in Fig. 5 are obtained. The displacement solutions of the PD-FEM coupled model with and without TE are compared with the analytical results. The results show that before node 4, the displacement of both the models are consistent with the analytical solution, indicating that the mechanical behaviour of the FEM elements in the coupled model remains unaffected. However, after passing node 4, the displacement of the model without TE begins to deviate from the analytical solution, indicating the presence of coupling effects at the interface. In contrast, the displacement of the model with TE completely matches the analytical solution, demonstrating that the proposed framework based on TE effectively resolves the coupling errors. This comparison highlights the influence of TE on the accuracy and continuity of the coupled model.

Table I: Parameters for the 1D coupled model.

Two-node linear rod element			**Peridynamics element**		
Young's modulus	Poisson's ratio	Cross-sectional area	Node spacing	Peridynamics horizon	Micromodulus
E (Pa)	υ	A (mm²)	Δ (mm)	δ (mm)	c (N/mm^{18})
1	0.3	1	1	2	0.5

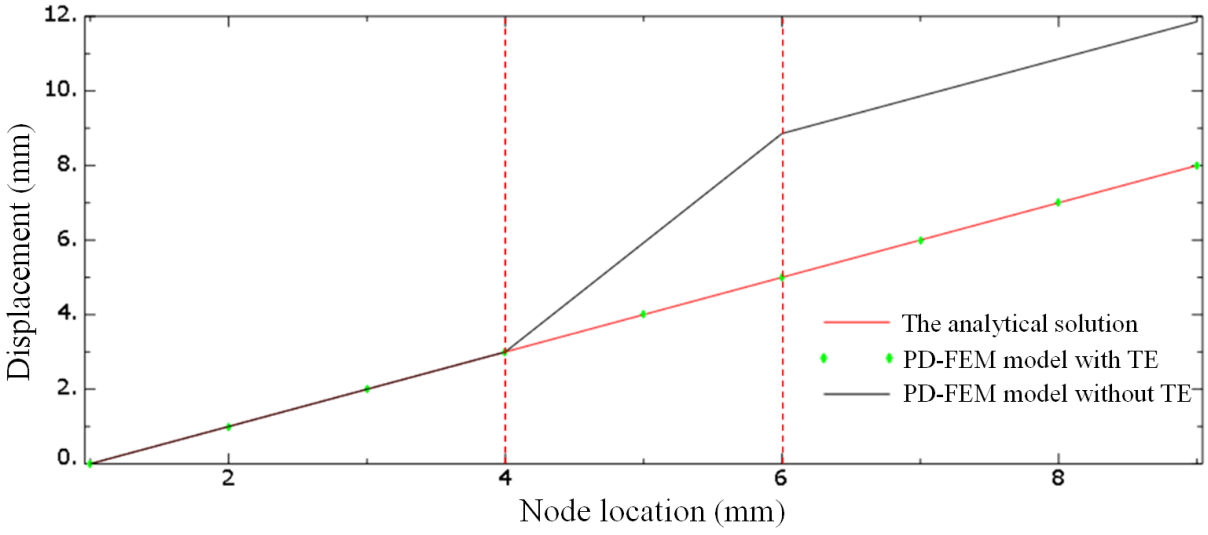

Figure 5: Comparison of displacement solutions of the PD-FEM coupled model with and without TE.

Additionally, the computation time required for the PD-FEM, PD, and FEM method when calculating a same 1D model with 31 nodes is compared, as shown in Table II. The time required by the PD-FEM method falls between the two, with the computation speed improved by approximately 20 % compared to the pure PD model. Indeed, as the proportion of FEM elements in the PD-FEM model increases, the computation time of the PD-FEM model will gradually approach to the pure FEM model, showing higher computational efficiency compared to the PD model. This trend indicates that the PD-FEM coupled model not only effectively addresses the boundary effects but also improves computational efficiency.

Table II: Comparison of computation time for different methods.

Calculation method	**Calculation time** (s)
FEM (31 nodes)	0.1
PD-FEM (25 PD nodes, 6 FEM nodes)	0.24
PD (31 nodes)	0.3

The aforementioned results offer initial insights into the effectiveness and applicability of the proposed framework. For higher-dimensional problems, the specific form of the transitional element may also vary; however, the method for constructing transition elements described by Eq. (21) remains applicable. It is particularly worth emphasizing that, as demonstrated by the 1D case above, the coupling framework proposed in this study – based on TE – imposes no specific requirements on the type of finite elements or PD elements. This significantly broadens the applicability of the method and enhances its capability to address complex problems. However, it should be noted that the requirement for the structural boundaries to be within the FEM region may compromise the effectiveness of the model when cracks occur at or near the boundaries.

4. CONCLUSION

This study proposes a novel Transitional Element-based framework to enhance the coupling of Peridynamics (PD) and the Finite Element Method (FEM). By addressing interface inconsistencies and mitigating surface effects, the TE approach provides a computationally efficient solution for hybrid modelling of crack propagation and material failure. The method effectively improves computational accuracy while preserving the distinct advantages of both PD and FEM. Future work will focus on numerical validation through large-scale simulations and the integration of TE into commercial FEM software to extend its applicability in engineering practice.

ACKNOWLEDGEMENT

This work was supported by the Fundamental Research Funds for the Central Universities (Grant No. M21RC00070).

REFERENCES

[1] Silling, S. A. (2000). Reformulation of elasticity theory for discontinuities and long-range forces, *Journal of the Mechanics and Physics of Solids*, Vol. 48, No. 1, 175-209, doi:10.1016/S0022-5096(99)00029-0

[2] Wang, S. R.; Zhao, J. Q.; Wu, X. G.; Yang, J. H.; Liu, A. (2021). Meso-scale simulations of lightweight aggregate concrete under impact loading, *International Journal of Simulation Modelling*, Vol. 20, No. 2, 291-302, doi:10.2507/IJSIMM20-2-558

[3] Oterkus, E.; Oterkus, S. (2024). Recent advances in peridynamic theory: a review, *AIMS Materials Science*, Vol. 11, No. 3, 515-546, doi:10.3934/matersci.2024026
[4] Scabbia, F.; Zaccariotto, M.; Galvanetto, U. (2023). A new surface node method to accurately model the mechanical behavior of the boundary in 3D state-based peridynamics, *Journal of Peridynamics and Nonlocal Modeling*, Vol. 5, No. 4, 521-555, doi:10.1007/s42102-022-00094-1
[5] Khan, M. A. A.; Sheikh, A. K. (2018). A comparative study of simulation software for modelling metal casting processes, *International Journal of Simulation Modelling*, Vol. 17, No. 2, 197-209, doi:10.2507/IJSIMM17(2)402
[6] Han, F.; Lubineau, G. (2012). Coupling of nonlocal and local continuum models by the Arlequin approach, *International Journal for Numerical Methods in Engineering*, Vol. 89, No. 6, 671-685, doi:10.1002/nme.3255
[7] Yu, Y.; Han, F.; Li, Z.; Sun, Y.; Mei, Y.; Zhang, A. (2023). Element-based coupling modeling of peridynamics and classical continuum mechanics for dynamic brittle fracture, *International Journal for Numerical Methods in Engineering*, Vol. 124, No. 24, 5574-5595, doi:10.1002/nme.7362
[8] Pernatii, A.; Gabbert, U.; Naumenko, K.; Hesse, J.-T.; Willberg, C. (2023). A Penalty method for coupling of finite-element and peridynamic models, *Proceedings in Applied Mathematics and Mechanics*, Vol. 22, No. 1, Paper e202200151, 6 pages, doi:10.1002/pamm.202200151
[9] Galvanetto, U.; Mudric, T.; Shojaei, A.; Zaccariotto, M. (2016). An effective way to couple FEM meshes and Peridynamics grids for the solution of static equilibrium problems, *Mechanics Research Communications*, Vol. 76, 41-47, doi:10.1016/j.mechrescom.2016.06.006
[10] Zaccariotto, M.; Mudric, T.; Tomasi, D.; Shojaei, A.; Galvanetto, U. (2018). Coupling of FEM meshes with Peridynamic grids, *Computer Methods in Applied Mechanics and Engineering*, Vol. 330, 471-497, doi:10.1016/j.cma.2017.11.011
[11] Anicode, S. V. K.; Madenci, E. (2024). Direct coupling of dual-horizon peridynamics with finite elements for irregular discretization without an overlap zone, *Engineering with Computers*, Vol. 40, No. 1, 605-635, doi:10.1007/s00366-023-01800-3
[12] Ou, X.; Yao, X.; Han, F. (2023). An adaptive coupling modeling between peridynamics and classical continuum mechanics for dynamic crack propagation and crack branching, *Engineering Fracture Mechanics*, Vol. 281, Paper 109096, 18 pages, doi:10.1016/j.engfracmech.2023.109096
[13] Dong, H.; Wang, H.; Cai, Z.; Wang, W.; Liu, Y. (2023). An enhanced adaptive coupling strategy of peridynamics and finite element method via variable horizon approach for simulating quasi-static fracture problems, *Engineering Fracture Mechanics*, Vol. 290, Paper 109492, 18 pages, doi:10.1016/j.engfracmech.2023.109492
[14] Liu, Q.; Xin, X. J.; Ma, J. (2023). Adaptive coupling peridynamic least-square minimization with finite element method for fracture analysis, *International Journal of Fracture*, Vol. 240, No. 2, 119-141, doi:10.1007/s10704-022-00678-4
[15] Bobaru, F.; Foster, J. T.; Geubelle, P. H.; Silling, S. A. (2016). *Handbook of Peridynamic Modeling*, CRC Press, Boca Raton
[16] Liu, B.; Huang, Y.; Jiang, H.; Qu, S.; Hwang, K. C. (2004). The atomic-scale finite element method, *Computer Methods in Applied Mechanics and Engineering*, Vol. 193, Nos. 17-20, 1849-1864, doi:10.1016/j.cma.2003.12.037
[17] Huang, X.; Bie, Z.; Wang, L.; Jin, Y.; Liu, X.; Su, G.; He, X. (2019). Finite element method of bond-based peridynamics and its ABAQUS implementation, *Engineering Fracture Mechanics*, Vol. 206, 408-426, doi:10.1016/j.engfracmech.2018.11.048
[18] Madenci, E.; Oterkus, E. (2014). *Peridynamic Theory and Its Applications*, Springer, New York
[19] Logan, D. L. (2017). *A First Course in the Finite Element Method*, 6th edition, Cengage Learning, Boston